Advanced Biomedical Engineering
12: 37–50, 2023.

Original Paper

DOI:10.14326/abe.12.37

Efficiency of a Visual Search Explained by the Small-World Features of a Gaze Position Network

Yuxuan WANG,[*] Honami HASHIMOTO,[*] Taishin NOMURA,[**] Akira TSUKADA,[***] Yoshinobu MAEDA[*,#]

Abstract A visual search is implemented when the eye moves to find a target symbol amongst many other symbols (distractors). The efficiency of a visual search is described by Hick's law, which shows that the search time increases logarithmically as the number of symbols increases. In this paper, the efficiency of visual search was analyzed from the perspective of the network features of a conceptual 'unobservable' gaze position network superimposed on a monitor screen filled with many symbols (search array board). We assume that the gaze position does not move freely around the search array board, but rather moves in a way restricted to the unobservable gaze position network. First, we statistically verified that the artificial gaze position network designed from the data of visual search experiments have small-world features, and depends on the ratio of the saccades. Second, by implementing gaze step simulations on such small-world networks, we statistically verified that the simulation search times were close to those obtained from the experiments and also to the minimum search times. Thus, this study suggests that an efficient visual search can be explained by a small-world architecture hidden in the unobservable gaze position network and thus has to be artificially designed.

Keywords: saccade, Hick's law, discriminant analysis, clustering coefficient, spatial extent of attention.

Adv Biomed Eng. **12**: pp. 37–50, 2023.

1. Introduction

Finding a target symbol from amongst many distractors is called a visual search. This has been studied by many researchers who have set several different tasks and conditions for their search experiments. For example, Amor et al. showed multifractal behavior arising from sequential gaze behavior in searching for a target symbol [1], and modeled their strategies using saccade behavior [2]. Drew et al. [3] experimented on a combination of visual and memory searches, and found that increasing the number of target symbols to memorize decreased the efficiency of the visual search. Becker [4] found that the dwell time of the gaze was affected by distractors similar to the target symbol. Dewhurst et al. [5] focused on the similarity of scanpaths in a sequential number search task. Dube et al. [6] clarified that a visual working memory supported 'facilitation', which moves the gaze position to an object similar to the target symbol in the search array board, and that 'inhibition' keeps the gaze position away from the distractors. Watson et al. [7] examined the difference between 'looking' and 'seeing' in a visual search, and showed the latter passive strategy made a visual search more efficient than actively searching. Greene and Brown [8] looked at the saccadic influence on fixation duration, and suggested that post-saccadic influences should contribute more to fixation duration than pre-saccadic influences in a visual search.

Some studies related to the real world have also been reported. Wasaki et al. [9] investigated gaze patterns during driving a vehicle in several hazardous situations. Clarke et al. [10] asked whether an individual's strategy and performance in one search task correlates with how that person performs in two other different tasks. Schill et al. [11] conducted visual search experiments using videos instead of pictures. Wolfe [12] was interested in

This study was presented at the Symposium on Biomedical Engineering 2022, September, 2022.
Received on July 25, 2022; revised on October 17, 2022; accepted on December 18, 2022.

[*] Graduate School of Science and Technology, Niigata University, Niigata, Japan.
[**] Graduate School of Engineering Science, Osaka University, Osaka, Japan.
[***] National Institute of Technology, Toyama College, Toyama, Japan.
[#] 2–8050, Ikarashi, Nishi-ku, Niigata 950–2181, Japan.
E-mail: maeda@eng.niigata-u.ac.jp

how serial and parallel processes collaborate in a visual search, and considered a real search for multiple target symbols in a complex scene that occurs only once. Furthermore, Wolfe and Horowitz [13] proposed five factors that guide the gaze position to the target symbol during a visual search, such as guidance based on the history of prior searches. This is similar to audio guidance of appropriate landmarks to help visually impaired persons reach their destinations [14, 15].

In these visual searches, the movement of the eye must be such that it finds the target symbol swiftly, because this is beneficial to the activities of our daily lives [16]. According to Hick's law [17], the time required to make a decision, i.e., the search time required to find the target symbol, is linearly related to the logarithm of the number of distractors. This means that a visual search can be optimized, in the sense that a long period of time to find a target symbol is undesirable. If one knows the position of the target symbol in advance of the visual search, one can move the gaze position to it via the shortest scanpath. Otherwise, one will have to search randomly to find the target symbol. It is not yet clear what kind of random search is necessary to obtain an efficient visual search. The visual system extends from the retina to the visual cortex in the brain; hence a technique to find a target symbol within a short period of time may be acquired by training. We have studied the efficiency of visual searches based on the assumption that the efficiency can be estimated from eye movements, without the need to monitor the activity in the visual cortex [18–20].

The movements of the eye are roughly classified into two kinds; involuntary small fixational movements and voluntary saccades. These are identified by the gaze position interval, or gaze step [21] between two gaze positions, measured on a monitor screen filled with many symbols (search array board). Fixational eye movements, or relatively small gaze steps, contribute to the perception of the symbol under, or near, the gaze position, if it continues for at least 0.1 seconds [22, 23] (or approximately 0.5 seconds at the maximum [24]). Saccadic eye movements are useful when the participant can scan the whole area of a monitor screen filled with many symbols in a short period of time. Combinations of such fixational and saccadic gaze steps draw 'network-like' figures on the search array board, using nodes (gaze positions) and line segments between two nodes (gaze steps). The movement of the gaze position seems to be free, but it also seems to be restricted to such conceptual 'unobservable' networks in the background of the movement of the gaze position. The ability of a visual search to find the target symbol swiftly must be hidden somewhere in the unobservable gaze position network superimposed on the search array board. No study has yet been conducted, which hypothesizes that unobservable networks control the movement of the gaze position. Elucidation of such networks may also be useful to reveal the efficiency of the visual search.

The main purpose of this study was to examine the efficiency of visual searches, using such unobservable gaze position networks from the viewpoint of complex network science. Several networks observed in human societies, such as electric power grids, epidemics, the brain, and IoT [25–30] are known to possess 'small-world' features. This means that the distance between two arbitrary nodes in the network are separated by only six degrees on average, even as the size of the network gets larger. A requirement for a small-world network is that two criteria should be simultaneously satisfied [27]. One is a global criterion reducing the actual large world to the small world by long line segments, or shortcuts, between nodes. The other is a local criterion gathering several nodes together as a cluster, which is composed of adjacent nodes connected by short line segments. If a network is small-world, then the distance between two arbitrary nodes is short and any node is clustered among nearest neighbors. We assert, as presented for the first time in this paper, that the small-world features of the unobservable gaze position network must be related to the efficiency of the visual search, through both a quick scan by the global criterion and accurate recognition by the local criterion.

We have considered, so far, the possibility of using a simple one-dimensional network [18]. Additionally, by calculating the Hurst exponent [31–33], we argued that the change in the temporal structure of the gaze steps during a visual search is scale invariant [19]. Furthermore, we confirmed that the mean two-dimensional network on the search array board designed from the visual search experiments became a small-world network [20]. However, three issues in our previous study remained to be resolved: 1) the study did not include a statistical analysis; 2) the minimum gaze step magnitude was set at 1 millimeter by rounding up, so that the fixational fluctuations on the search array board were relatively more marked than the experimental results; and 3) saccades were defined conventionally as eye velocities of 30 deg/s or greater, so that the classification of saccades did not reflect individual differences between the participants, such as some having relatively smaller gaze steps than others. In this paper, we address the above three issues, and prove that the efficiency of a visual search is derived from the small-world features hidden in the gaze position network (actual two-dimensional network). Specifically, 1) we identified networks that were not statistically different from small-world networks; 2) we set

the minimum gaze step magnitude at 0 by rounding, i.e., a magnitude of 0 denotes that the gaze position stays on the node of the network for a certain length of time; and 3) we determined the threshold that differentiates fixational from saccadic gaze steps by versatile discriminant analysis (see **Section 3.1**). Thus, an artificial gaze step model moving on the gaze position network satisfactorily reproduced the real gaze steps obtained from visual search experiments.

First, the visual search experiments are described (**Sections 2 and 3**) in which every participant found one target symbol out of many distractors as swiftly as possible. Second, using data obtained from the experiments and applying the Watts and Strogatz's algorithm [27], we designed several gaze position networks (**Section 4**). We statistically verified that some of them had small-world features (**Section 5**). Finally, we propose that visual search simulations using an artificial gaze step model on the small-world network explain the short search times obtained from the experimental data (**Section 6**).

2. Methods of Visual Search Experiment

The experiment was performed in accordance with the Declaration of Helsinki, and was approved by the ethics research committee of Niigata University (No. 3005). Informed consent was acquired from all the participants prior to their participation.

2.1 Design, Task, and Participant

The visual search experiments were performed using monocular recording (the right eye) with an iView X^{TM} Hi-Speed (SensoMotoric Instruments, Teltow, Germany) operating at an acquisition frequency of 500 Hz (0.002 seconds). The participant sat 600 mm away from the monitor screen and his behavior was assessed through the keyboard. We obtained precise gaze position data from the movements of the eye using a jaw-receiving stand. The experiment was conducted under an average environmental illuminance of 270 lx. The task presented to the participant was to find only one target symbol as swiftly as possible from an array presented on a 23-inch monitor (horizontal: 1920 pixels or 524 mm, vertical: 1080 pixels or 295 mm).

The array consisted of 256 (16 × 16) different randomly allocated symbols comprising Gothic-type symbols; Arabic, Greek and Chinese numerals; mathematical symbols; letters from Roman, Greek, Cyrillic (Russian) and Kannada (Indian) alphabets; Hiragana and Katakana (Japanese), and other special characters. We tried to incorporate symbols with both many and few random strokes. Moreover, we incorporated readable (Hiragana, numbers, etc. for Japanese participants) and unreadable (Cyrillic and Kannada) characters in equal proportion as far as possible. However, similar symbols were not used, such as the capital letter "O" and the number "0". All the symbols were 8 mm × 8 mm in size and presented in black on a white background. The distance between two symbols was also 8 mm. To break the regular alignment, the relative position of each symbol was shifted randomly by a maximum of 50% up, down, left or right from the central position, as shown in **Fig. 1(a)**. The total size of the search array board was approximately 256 mm × 256 mm.

Sixteen male university students (age 22.7 ± 0.9) participated in the experiments. Each participant repeatedly performed 6 trials. In one trial, the target symbol was first presented in the central position on the monitor screen to be memorized by the participant, and then the search array board was presented to the participant by depressing the space key. Therefore, at the beginning of each trial, every participant was supposed to fix his eyes onto the central position of the monitor screen. The positions of the 256 symbols including the target symbol were randomly changed for each trial. We also intentionally set the search array board without the target symbol

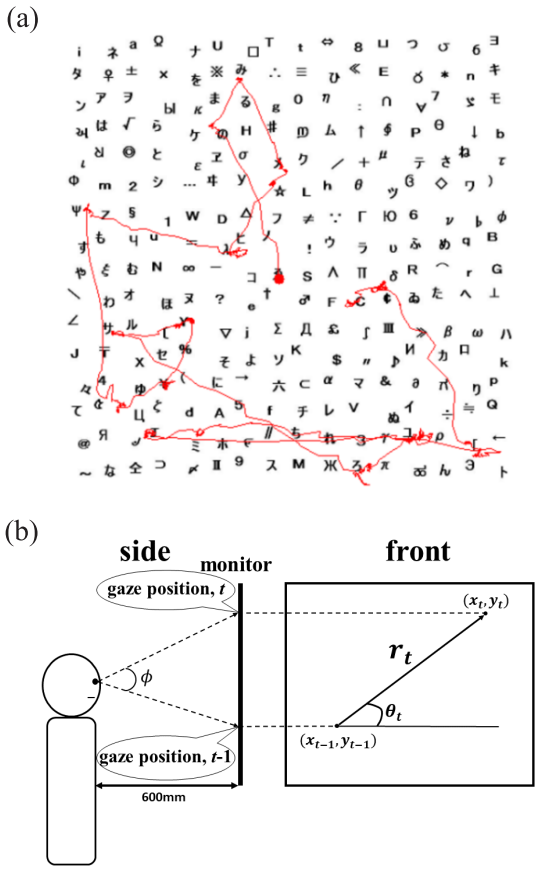

Fig. 1 (a) An example of a search array board and the measured scanpath of the gaze position. (b) Conceptual diagram of the gaze step magnitude r_t, its angle θ_t, and the drift angle of eye movement ϕ.

in 2 arbitrary trials, i.e., 'dummy trials.' The remaining 4 trials were 'ordinary trials' with the target symbol. All trials were forcibly terminated after 60 seconds, regardless of whether it was a dummy trial or the participant did not find the target symbol in an ordinary trial. When finding the target symbol, the participant indicated it by depressing the space key.

2.2 Data Preprocessing

The output data are the search time resolved into 0.002-second steps, the diameter of the pupil in the eye, and the gaze position (u_t, v_t) in pixels at time t. When the diameter of the pupil was not measured correctly (for example due to eye blinks), the corresponding data were all removed from analysis because of incorrect gaze positions. In order to obtain the converted gaze position (x_t, y_t) in millimeters, we used the following transformations:

$$x_t = 524\, u_t \,/\, 1920, \tag{1}$$

$$y_t = 295\, v_t \,/\, 1080, \tag{2}$$

where 1 pixel corresponds to approximately 0.03 degrees of the drift angle, and 1 mm to approximately 0.1 deg. The gaze step magnitude r_t in millimeters at time t between (x_t, y_t) and (x_{t-1}, y_{t-1}) was calculated using the following equation:

$$r_t = \sqrt{(x_t - x_{t-1})^2 + (y_t - y_{t-1})^2}. \tag{3}$$

The r_t in eq. (3) is processed as follows:

$$\overline{r_t} = (r_{t-2} + r_{t-1} + r_t + r_{t+1} + r_{t+2})\,/5, \tag{4}$$

$$\gamma_t = \lfloor \overline{r_t} + 0.5 \rfloor. \tag{5}$$

The $\overline{r_t}$ in eq. (4) represents a simple moving average of r_t in eq. (3). This smoothing is adopted to reduce noise. The integer γ_t in eq. (5) represents quantization for $\overline{r_t}$ by means of rounding off, where $\lfloor \cdot \rfloor$ represents a mathematical floor function.

The direction of r_t on the monitor screen is described by the angle θ_t, which is sampled every 1 degree by rounding off. θ_t is measured in a counter-clockwise direction from the right-hand side of the screen, where $\theta_t = 0$ [**Fig. 1(b)**]. After simple moving average, the angle θ_t at time t is associated with γ_t at time t. In the next section, we select several data that are necessary to design gaze position networks, and derive an artificial gaze step model from the visual search experiments to be used in the visual search simulation.

3. Results of the Visual Search Experiment

The results of the dummy trials are presented in **Section 3.1**. The results of the ordinary trials are presented in **Section 3.2**. An example of the measured scanpath of the gaze position is shown in **Fig. 1(a)** as a red line.

3.1 Dummy Trials

In the dummy trial, we obtained about 30000 sequential measurements of the gaze step magnitude r_t in the maximum trial time of 60 seconds with sampling period of 0.002 seconds. Sixteen dummy trials randomly selected from all participants were analyzed. The γ_t calculated from eqs. (4) and (5) were classified either as fixational or saccadic line segments. Bao et al. [20] identified the saccadic line segments as those with drift angular velocity greater than 30 deg/s, which is a conventionally used method [34–36]. Other studies used neural networks [37] and intelligent tools [38] to classify fixations and saccades. In this paper we classified γ_t into either fixational or saccadic line segments using the versatile discriminant analysis proposed by Otsu [39], which was originally applied to the binarization of gray scale images. Otsu's discriminant analysis has the advantage that the threshold that differentiates between the fixational and saccadic line segments is calculated based on each trial.

Let N be the total number of γ_t values, and n_l be the number that satisfies $l - 1 < \gamma_t \le l$, i.e., every γ_t is quantized by a natural number l (the maximum value is denoted by l_{max}). Then a threshold l^* ($< l_{max}$) is determined at which the variance between the fixational and saccadic line segments is the highest. The variance σ^2_{FS} is given by

$$\sigma^2_{FS}(l^*) = \left\{ N_F\,(\mu_F - \mu_T)^2 + N_S\,(\mu_S - \mu_T)^2 \right\} /N, \tag{6}$$

where $N_F = \sum_{l=1}^{l^*} n_l$ and $N_S = \sum_{l=l^*+1}^{l_{max}} n_l$ are the numbers of fixational (suffix F) and saccadic (suffix S) line segments, respectively, and $N_F + N_S = N$. The two mean values μ_F and μ_S are given by $\mu_F = \sum_{l=1}^{l^*} l n_l / N_F$ and $\mu_S = \sum_{l=l^*+1}^{l_{max}} l n_l / N_S$, respectively. The total mean value μ_T is given by $\mu_T = \sum_{l=1}^{l_{max}} l n_l / N$.

For example, the sequence of γ_t data obtained from one of the participants is shown in **Fig. 2(a)**, and the histogram is given in **Fig. 2(b)**. The threshold classifying the saccadic from the fixational line segments is determined to be $l^* = 2$, because the maximum variance obtained using eq. (4) is $\sigma^2_{FS}(l^*) \cong 0.8$ at $l^* = 2$, which is shown in **Fig. 2(c)**. In this trial (or for this participant), we identified the fixational line segments to be under 2 mm; therefore, the saccadic line segments were evaluated as being over 3 mm. Similarly, γ_t values from other trials were also classified into either fixational or saccadic line segments. For almost all trials, l^* was 2 mm, and the maximum and minimum values were 3 mm and 1 mm, respectively.

Both types of line segments did not appear at random, i.e., the behavior was temporal with a large Hurst exponent [31–33], apart from normal Brownian motion. They appeared consecutively for a certain period of time. In general, one saccade is considered to last at least 0.02 seconds, i.e., it is formed from at least 10 saccadic line

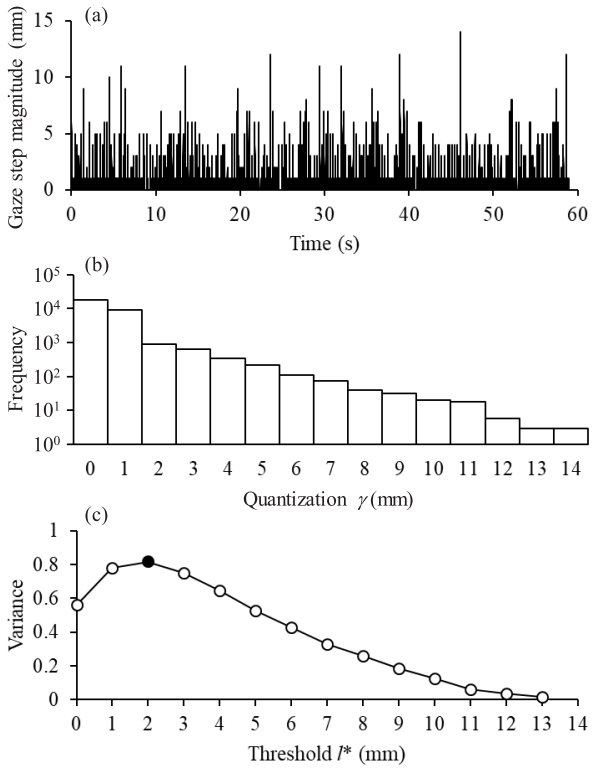

Fig. 2 (a) Temporal sequence of the quantized gaze step magnitudes γ_t. (b) Histogram of γ data with l_{max} = 14. (c) Variance σ^2_{FS} (l^*). The maximum value is at l^* = 2. This means that γ_t less than 2 mm should be regarded as fixational line segments.

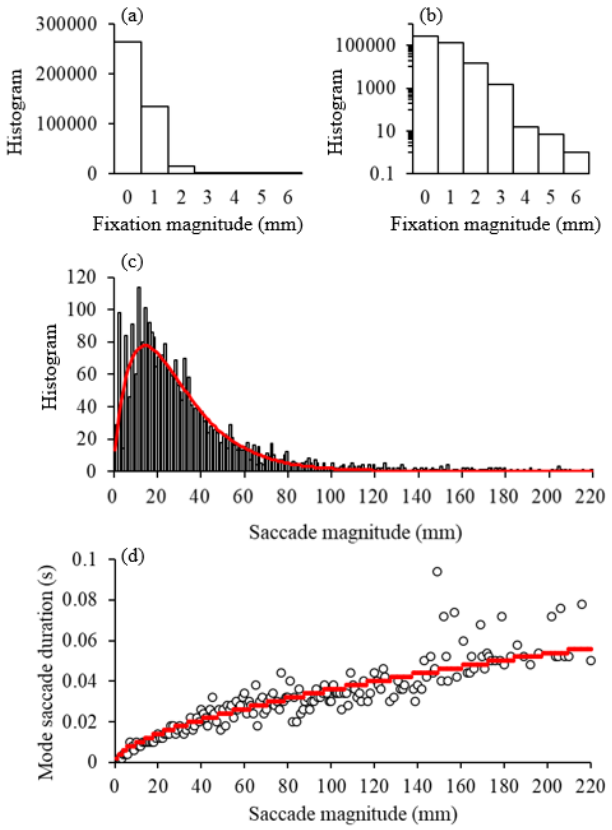

Fig. 3 Histograms of fixation magnitude with (a) a linear ordinate and (b) a logarithmic ordinate. (c) Histogram of saccade magnitude. (d) Mode saccade durations for given saccade magnitudes. The red curve is an approximate curve.

segments in the experiments measured with a sampling frequency of 500 Hz (or 0.002 s). In this paper, one saccade was formed as a straight line connecting the start and the end points, for all consecutive saccadic line segments lasting more than 0.02 seconds. Therefore, the magnitude of one saccade, R, is generally less than $\sum_{t=1}^{d_s/0.002} \gamma_t$, where d_s represents the saccade duration (consecutive saccadic line segments). For less than 10 consecutive saccadic line segments, we considered this to be a saccade only when the magnitude of the straight line from the start to the end points was above the threshold l^*. Otherwise, these line segments were interpreted as fixational ones. Similar to the saccade extraction process, less than 10 consecutive fixational line segments between two saccades were interpreted as errors; in this case, we omitted the fixational line segments (error) and combined the two saccades on both sides of the error into one large saccade. In this paper, therefore, some fixations were composed of more than 10 consecutive line segments, or longer than 0.02 seconds.

Figure 3(a) shows a histogram of the frequencies of the magnitudes of all the fixational line segments for the 16 participants. **Figure 3(b)** shows the data in **Fig. 3(a)** with the vertical axis changed to a logarithmic scale. The magnitudes were less than 3 mm from Otsu's discriminant analysis, but line segments with relatively large magnitudes greater than 4 mm were also obtained as fixational line segments that did not pass the saccade extraction process, as mentioned above. The frequencies of appearance were 63.55% for 0 mm, 32.45% for 1 mm, 3.64% for 2 mm, 0.35% for 3 mm, and less than 0.01% for others. Approximately two-thirds were 0 mm, and they were interpreted as not moving. Almost all the remaining one-third were classified as 1 mm (moving a little). In the design of the gaze position network in **Section 4**, fixational line segments from 1 to 6 mm, based on the histogram in **Fig. 3(b)**, are used. On the other hand, the percentage of line segments at '0 mm' (63.55%) was used as the probability that the artificial gaze step model stays on the node of the gaze position network in the visual search simulation (see **Section 4**).

Figure 3(c) shows a histogram of the frequencies of the magnitudes of all the saccades for the 16 participants, where the abscissa represents the saccade magnitude, R. The most frequent magnitude was approximately 20 mm. Although there were individual differences in the data, it

did not make sense to categorize the distribution by individual differences based on the number of participants in this study. Therefore, we considered the individual differences to be errors and expressed them as a single distribution. The red curve, L_s, is approximated by the following function:

$$L_s = 14.4R\exp(-0.068R). \quad (7)$$

Equation (7) is used in designing the gaze position network (see **Section 4**).

Figure 3(d) shows the relationship between the saccade magnitude and the saccade duration. The ordinate represents the mode saccade duration for a given saccade magnitude on the abscissa. This represents, in a sense, the main sequence [40] that is often applied to the relationship between the duration or peak velocity and the saccade magnitude. The red curve D_s is approximated by the following function:

$$D_s = 0.0023R^{0.592}, \quad (8)$$

where the values of the ordinate are quantized every 0.002 seconds. In this paper, this function [eq. (8)] is used to determine the time that the artificial gaze step model moves on the saccade of the gaze position network (see **Section 6**).

Figure 4(a) and (b) shows histograms of the frequencies of the angles of all the fixational line segments and the angles of all the saccades, respectively. When designing a gaze position network, line segments of 1 mm are set to 8 neighboring nodes (see **Section 4**) as the first reference network. Therefore, the distribution of fixational line segments greater than 2 mm in magnitude only were used in the histogram, and the line segments of 0 mm and 1 mm were excluded in **Fig. 4(a)**. Although the directions of the fixational movements were mostly up and down, those of the saccades were mostly right and left as shown in **Figs. 4(a) and (b)**. Approximate functions, A_f and A_s, for the red curves shown in **Figs. 4(a) and (b)**, respectively, are given in eqs. (9) and (10),

$$A_f = \frac{1700\times34}{\alpha^2+34^2} + \frac{1300\times12}{(\alpha-90)^2+12^2} + \frac{1700\times34}{(\alpha-180)^2+34^2} + \frac{1300\times12}{(\alpha-270)^2+12^2} + \frac{1700\times34}{(\alpha-360)^2+34^2}, \quad (9)$$

$$A_s = 4.8\cos\left(\frac{2\pi}{180}\alpha\right) + 4.9\cos\left(\frac{4\pi}{180}\alpha\right) + 9.1, \quad (10)$$

where α is the angle in degrees. These are used in designing the gaze position network (see **Section 4**).

The ratio q, which is the number of saccades to the total number of line segments composed of saccades and fixational line segments except for $l = 0$, measured in the 16 trials of the visual search experiment was calculated to be $q \cong 0.021 = q_{\exp}$ (suffix 'exp' signifies that it is an experimental value). Fixational line segments, '$l = 0$,' were excluded because these do not appear as line segments in the gaze position network.

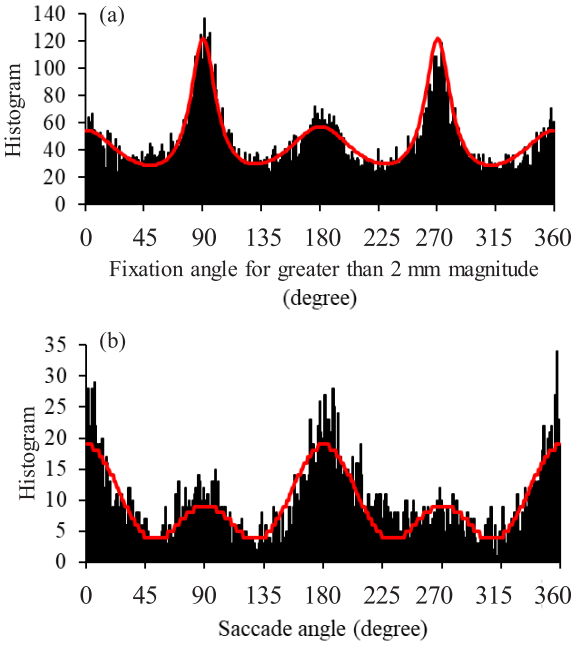

Fig. 4 (a) Histogram of fixation angles with magnitudes greater than 2 mm. (b) Histogram of saccade angles. Red curves represent approximate curves.

3.2 Ordinary Trials

From the ordinary trials, we also obtained the search time. Of the 64 trials (4 trials per participant, and 16 participants in total), valid data for analysis was obtained in 57 trials. The search times for these trials were all greater than 1 second. The median search time was approximately 11.8 seconds, and we used this value in the visual search simulation (see **Section 6**). The remaining 7 trials were classified as measurement failures, due to failure to find the target symbol. The search time for these trials was 60 seconds.

Figure 5 shows an example of the variation in distance from the gaze position to the center of the target symbol. Constant values and rapidly changing movements represent fixations and saccades, respectively. In order to find the target symbol, the extent of perception must be defined. In general, the requirement for perception is that the gaze must remain stationary for at least 0.1 seconds [22, 23]. Moreover, peripheral vision is known also to contribute to perception [41–46]. Some researchers [42–44] have reported that central vision and peripheral vision are mutually and intricately related, but others [45] report that the peripheral vision does not have much impact on the search performance. In a visual search, therefore, knowledge of the peripheral vision may be underutilized. In finding target symbols, Wu and Wolfe [47] classified the visual field into three types: res-

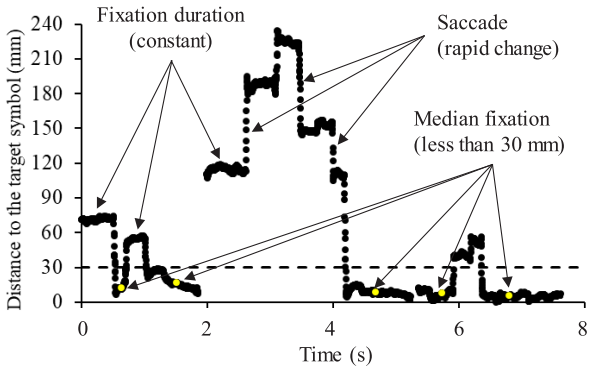

Fig. 5 Distance from the gaze position to the center of the target symbol (one example). The spatial extent of attention is shown as a region smaller than 30 mm. The five yellow circles in the fixation duration are median values.

olution (on the target), attentional (near the target), and exploratory (far from the target), and showed why visible targets can be clearly missed, especially in the latter two types. Focusing on the attentional visual field (or the spatial extent of attention [48, 49]) in the present study, we consider the following two parameters that contribute to finding of the target symbol. One is the distance between the center of the target symbol and the current node of the gaze position. The smaller this distance, the more likely one is able to find the target symbol. The other is the fixation duration remaining within the spatial extent of attention. The longer this duration, the easier the target symbol can be found. In our experiments, when the radius of the extent of attention was greater than 30 mm, the participants hardly ever found the target symbol. Thus, in the visual search simulation in **Section 6**, the extent of attention was set at a radius less than 30 mm. The spatial extent of attention is shown by the horizontal dashed line illustrated in **Fig. 5**. There were a total of five fixation durations, the median of which is shown by the yellow circles. In only the last fixation duration, the participant successfully found the target symbol.

The total number of fixation durations in the spatial extent of attention obtained from the 16 study participants was 152, 42 of which led to the discovery of the target symbol. **Figure 6(a)** presents the mean distance to the target symbol, δ in mm, for the non-finding and finding cases. **Figure 6(b)** shows the mean fixation duration, τ in seconds, for the non-finding and finding cases. The vertical bars represent the standard deviations in both graphs. We verified that δ was shorter [**Fig. 6(a)**] and τ was longer [**Fig. 6(b)**] when the target symbol was found. These two variables were integrated into one variable to produce the finding index, φ in s/m. This is given by the following;

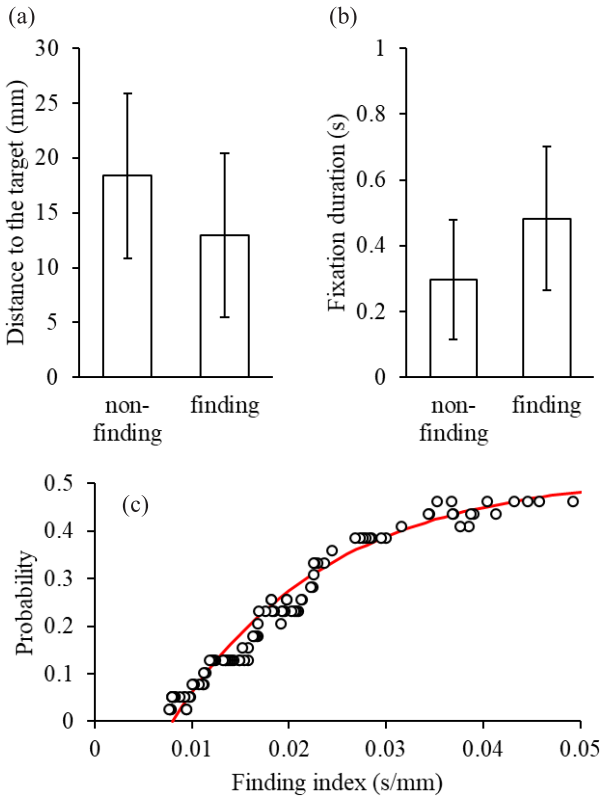

Fig. 6 (a) Mean distances to the target symbol from the gaze position and (b) mean fixation durations for non-finding and finding cases. (c) Probability of finding a target symbol for given finding indices φ. The red curve represents an approximate curve.

$$\varphi = \frac{\tau}{\delta}. \tag{11}$$

It is clear from eq. (11) that a combination of long fixation duration τ and short distance δ to the target symbol results in a large finding index φ. When the finding indices are arranged in descending order, the greater the value of φ, the easier the target symbol is found. Let label 1 be assigned when the target is found, and label 0 when the target is not found in descending order of φ. Then, we can obtain the probability ρ of finding a target symbol by a simple moving average for φ in descending order, as follows:

$$\rho(\varphi_k) = \sum_{i=k-19}^{k+19} U(\varphi_k)/39, \tag{12}$$

where φ_k represents the finding index for the k-th φ arranged in descending order. $U(\varphi_k)$ is given by

$$U(\varphi_k) = \begin{cases} 1, & \text{finding} \\ 0, & \text{non-finding} \end{cases}. \tag{13}$$

The plots in **Fig. 6(c)** show the probability ρ of finding a target symbol for the finding index φ_k. The red curve is an approximate curve given by the following equation,

$$\bar{\rho}(\varphi_k) = \begin{cases} 0.52\left\{1-\exp\left(-\dfrac{\varphi_k - 0.008}{0.016}\right)\right\}, & \varphi_k > 0.008, \\ 0, & \varphi_k \le 0.008. \end{cases} \quad (14)$$

Equation (14) is used in the visual search simulation (see **Section 6**) as the probability of finding a (virtual) target symbol.

4. Design of a Gaze Position Network

Using the experimental results of the dummy trial, we constructed a gaze position network. We superimposed 65536 (256×256) nodes at 1 mm intervals on the search array board. First, every node was coupled with 8 other adjacent nodes with '1 mm' fixational line segments. By the boundary conditions, the total number was 260610. Then, fixational line segments from 2 to 6 mm were probabilistically added to the above network based on the frequency of appearance [**Fig. 3(b)**] and the angle [**Fig. 4(a)**, or eq. (9)]. If the tip of the fixational line segment did not end with a node, it was connected to the node nearest to the tip. Note that only one line segment is allowed between two nodes.

Next, we exchanged some of the fixational line segments selected at random with saccades, using the histograms in **Fig. 3(c)** [eq. (7)] and **Fig. 4(b)** [eq. (10)]. By replacing one fixational line segment with one saccade, the total number of segments (including saccades) was kept constant. The ratio of the number of saccades to the total number of line segments, q, is a parameter used to design gaze position networks. A smaller value of q implies that it is closer to a regular network composed of almost all fixational line segments, whereas a greater value of q signifies a network closer to a random graph composed of almost all saccades. The network that appears when $q = q_{\mathrm{exp}} \cong 0.021$ should be a real visual search. The saccade angle, θ_s, is probabilistically extracted from the histogram in **Fig. 4(b)** [eq. (10)]. Similarly, the saccade magnitude R is extracted from the histogram in **Fig. 3(c)** [eq. (7)]. Then the saccade is drawn in the direction θ_s with magnitude R, and is coupled to the node nearest to the tip. If the tip of the saccade is outside the search array board, the angle θ_s is re-extracted from **Fig. 4(b)** [eq. (10)] until a valid θ_s is obtained.

This procedure of replacement of the fixational line segment with a saccade was iterated until the current ratio $\hat{q}$ of the saccades was above the preset q. Then, the gaze position network was completed with the ratio $\hat{q}$, where $\hat{q}$ is nearly equal to but usually greater than q. Stochastically designed gaze position networks are different, but any network is a sample with an unbiased estimator Q of the ratio $\hat{q}$, where Q is the random variable that satisfies the expectation $E(Q) = \hat{q} \cong q$.

5. Verification of a Small-World Network

5.1 Two Parameters

As the ratio q increases, the network generally changes from a locally coupled regular network to a small-world network, and finally to a random network [27]. There are two parameters to evaluate whether or not the network is a small-world network. One is a clustering coefficient at a randomly selected node i, denoted by $C_i(q)$, and the other is a weighted minimum distance between node i and another node, denoted by $L_i(q)$. $C_i(q)$ is derived from m_i, which is the number of triangles constructed by coupling with two other nodes that have a path with node i, and is expressed as follows:

$$C_i(q) = \frac{m_i}{\binom{k_i}{2}} = \frac{2m_i}{k_i(k_i-1)}. \quad (15)$$

$L_i(q)$ is calculated using the Dijkstra algorithm [50]. The weight of the line segment represents the time for which an artificial gaze step model moves, as described in **Section 6**. This value is obtained from **Fig. 3(d)** [eq. (8)].

In this paper, we randomly selected 1000 nodes for every q. The median $C_i(0)$ and $L_i(0)$ at $q = 0$ were $\bar{C}(0) \cong 0.429$ and $\bar{L}(0) \cong 0.178$, respectively, which are estimated as the maximum values. Then, the gaze position network is a locally coupled network composed of only fixational line segments. $C_i(q)$ and $L_i(q)$ have the same dimensions if they are normalized by their maximum values. The difference $h_i(q)$ between $C_i(q)$ and $L_i(q)$ normalized by $\bar{C}(0)$ and $\bar{L}(0)$, respectively, is defined by

$$h_i(q) = C_i(q)/\bar{C}(0) - L_i(q)/\bar{L}(0). \quad (16)$$

From eq. (16), a small-world feature is observed when both the large clustering coefficient necessary for accurate recognition and the short distance between arbitrary positions of the network necessary for rapid scan are satisfied. In other words, the small-world network appears at a relatively large value of $h_i(q)$.

5.2 Statistical Test

Figure 7(a) shows the relationship of median $C_i(q)/\bar{C}(0)$ (denoted by circle) or median $L_i(q)/\bar{L}(0)$ (denoted by triangle) with respect to q on a logarithmic scale, where the symbol x represents the value at $q \cong q_{\mathrm{exp}}$. Both values are close to 1 in the neighborhood of small q. As q increases, the weighted minimum distance (triangle) decreases before the clustering coefficient (circle) does in the range of $q < 0.2$. It is presumed, therefore, that median $h_i(q)$, denoted by $\bar{h}(q)$, possesses only one maximum point. If the network satisfies both conditions of large clustering coefficient and small weighted minimum distance, $\bar{h}(q)$ becomes so large that it is known as a small-world network [27]. Therefore, $\bar{h}(q)$ is an important index to evaluate whether a network architecture has

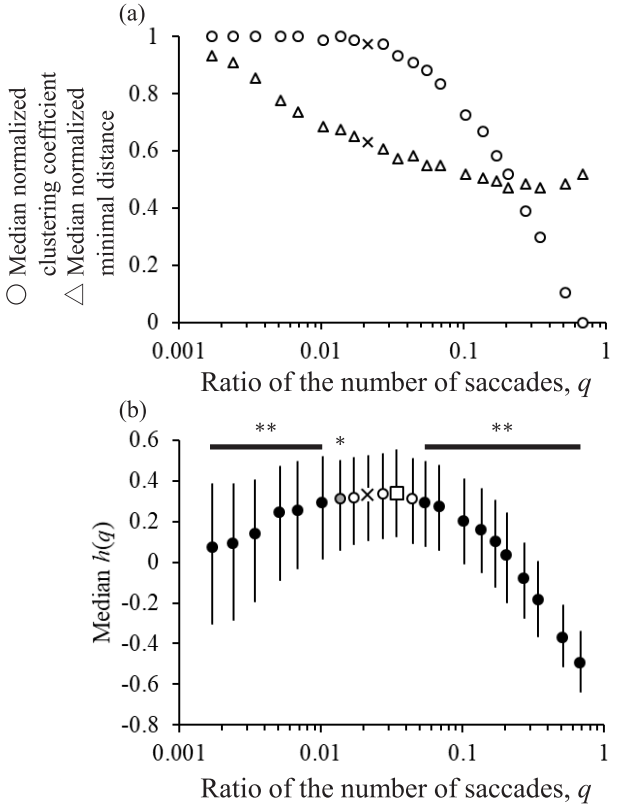

Fig. 7 (a) Median normalized clustering coefficients (circles) and median normalized weighted minimum distances (triangles) for given q values. The symbol × represents the value at $q \cong 0.021 \cong q_{\exp}$. (b) Median $h_i(q)$ (denoted by $\bar{h}(q)$). The non-filled square represents the maximal $\bar{h}(q)$ ($\bar{h}(q) \cong 0.34$), and the filled circles and the gray circle represent significant differences compared with the maximum (Steel's test, $p < 0.01$ and $p < 0.05$, respectively). The range of $0.014 < q < 0.044$ was found to be not significant (three non-filled circles and one cross).

small-world features.

In **Fig. 7(b)**, $\bar{h}(q)$ is plotted against q between 0.002 and 0.683 on a logarithmic scale, where the vertical bars represent quartile deviations. The maximum $\bar{h}(q) \cong 0.337$ occurs at $q = q_{\max} \cong 0.034$, as illustrated by the square. By comparing with the maximum value using one-sided Steel's test, one gray-filled circle and all black circles were found to be significantly different ($p < 0.05$ and $p < 0.01$, respectively), while four values of $\bar{h}(q)$ in the range $0.017 < q < 0.044$ were not significant (i.e., they possessed small-world network features). The experiment value (symbol x, $q_{\exp} \cong 0.021$) was contained within this range, indicating that the actual gaze position is expected to move over a small-world gaze position network. The method of analysis in this paper is different from the previous work [20] and the ratio of the number of saccades changes from 0.043 [20] to 0.021, but both experimental values are within the small-world range of $0.017 < q < 0.044$, i.e., the results are not affected by the analytical method.

6. Visual Search Simulation

6.1 Method of Simulation

Next, we simulated a visual search on several gaze position networks using an artificial gaze step model. We place the gaze step model at the start node closest to the center of the gaze position network. In addition, we established a virtual target symbol in a randomly selected location within a square area with $8 \times 8 = 64$ nodes. First, the gaze step model probabilistically determines whether to stay in the same place (63.55% probability estimated for 0 mm in **Section 3.1**) or to move (the remaining 36.45% probability). The simulation time required is 0.002 seconds (sampling period) even if the gaze step model stays on the node. In the case of moving, the gaze step model moves randomly to the next node on the fixational line segment every 0.002 seconds, while searching for the virtual target symbol. From the experiment described in **Section 3.2**, we set that at least 1 second is needed for discovery of the virtual target symbol. When the gaze step model reaches a node coupled with saccades, it moves preferentially on one of the saccades for d_s seconds which is estimated from **Fig. 3(d)** [eq. (8)]. After the saccades, the gaze step model moves on fixational line segments again for at least 0.02 seconds, until reaching the next node coupled with saccades.

When the virtual target symbol is in the spatial extent of attention (radius of 30 mm, refer to **Section 3.2**) of the artificial gaze step model, it is detected with a probability of finding the virtual target symbol [**Fig. 6(c)** or eq. (14)]. This check is performed every time the gaze step model moves over a node until the virtual target symbol is out of the spatial extent of attention. From the monotonic increase in **Fig. 6(c)** [eq. (14)], the greater the finding index becomes, the more easily the virtual target symbol is found. In other words, the longer the fixation duration and the smaller the distance between the gaze position and the virtual target symbol, the more easily the virtual target symbol is detected. Note here that the ease of finding the virtual target symbol depends on the form of eq. (14).

In the visual search experiment, the participant receives not only perceptual 'local' information about whether the symbol he is currently looking at is the target symbol, but also navigational 'global' information about where the current gaze position is located on the search array board. Especially, the latter information is important to search evenly on the search array board. In order to design global information on the artificial gaze step model, we adopted a random way-point search. An

arbitrary position was selected at random as a temporary destination. If the artificial gaze step model entered the spatial extent of attention (30-mm radius) of the waypoint, another temporary destination was newly set at another position. This operation was repeated until the virtual target symbol was found.

6.2 Results of Simulation

Figure 8 shows the scanpaths of typical experimental searches and artificial simulation searches. Some participants found the target symbol in approximately 21 seconds [**Fig. 8(a)**], whereas others found it in just 3 seconds [**Fig. 8(b)**]. **Figure 8(c)** is an artificial simulation search with $q = q_{\mathrm{exp}} \cong 0.021$ (about 15 seconds until found). **Figure 8(d)** is another artificial simulation search with $q = q_{\mathrm{max}} \cong 0.034$ (about 13 seconds until found). These four figures are similar but the difference between the experimental and artificial simulations is the saccades. In artificial simulations, the saccade is illustrated as a straight line (because saccadic line segments measured with a sampling frequency of 0.002 seconds are connected to a straight line in **Section 3.1**), whereas in the experiment the saccade is not always linear.

Figure 9(a) shows the median search time for every q (60 iterations ≅ 57, that are the valid data from the ordinary trials) when the position of the virtual target symbol was changed randomly for every iteration. The vertical bars represent quartile deviations. The label S.W. represents small-world networks evaluated in the experiment, as shown in **Fig. 7(b)**. By comparison with the maximum value ($q = q_{\mathrm{max}} \cong 0.034$, square labels) using one-sided Steel's test, the ranges of q shown by the single and double asterisks were found to be significant, i.e., $p < 0.05$ and $p < 0.01$, respectively (gray-filled and black-filled circles, respectively). This result means that as the value of q increases from the locally coupled gaze position network generating fixational eye movements, the search time decreases and is minimized at around 11.8 seconds where the network becomes small-world. **Figure 9(b)** shows the histogram of the experimental search time. Similarly, the histogram of the simulation search time for a random number q in the range of $0.017 < q < 0.044$ that satisfies the small-world condition ["S.W." in **Fig. 9(a)**] is shown in **Fig. 9(c)**. These histograms are slightly different but roughly similar, i.e., they show a monotonically decreasing trend with increasing search time. Therefore, this analysis confirmed that the efficiency of a visual search should be derived from the small-world features of the gaze position network. We clarified that the search time is relatively small when the gaze step model is simulated on the small-world network, and is also close to the experimental data.

However, even for greater values of q ($q > 0.034$), the search time remained constant. In other words, contrary to the authors' expectations, the search time was not

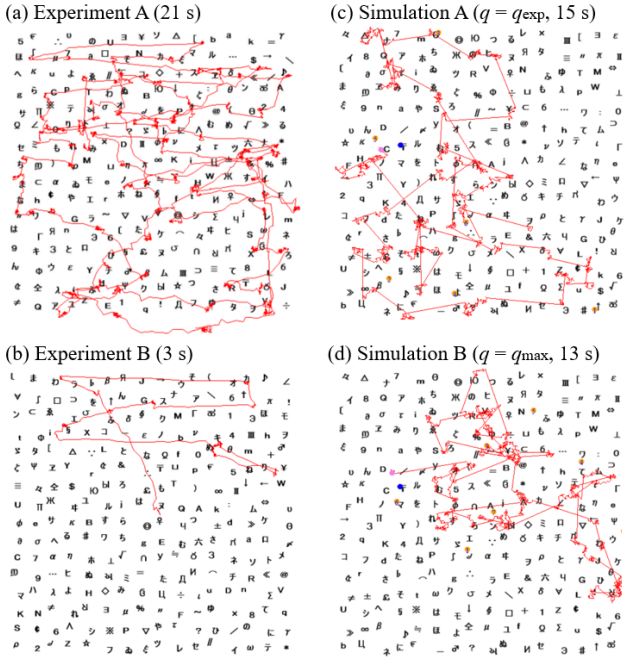

Fig. 8 Experimental searches finding target symbol (a) in 21 seconds and (b) in 3 seconds. (c) A simulation search ($q = q_{\mathrm{exp}} \cong 0.021$) finding target symbol in 15 seconds. (d) Another simulation search ($q = q_{\mathrm{max}} \cong 0.034$) finding target symbol in 13 seconds.

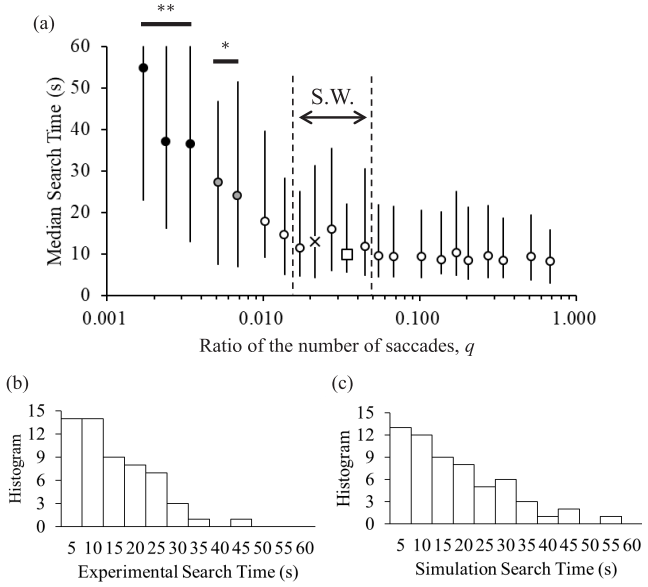

Fig. 9 (a) Median search time of a visual search simulation for given q values ($^{**}p < 0.01$, $^{*}p < 0.05$ by Steel's test). S.W. represents the region of the small-world network. (b) Histogram of experimental search time. (c) Histogram of simulation search time for a random number q in the range of the small-world.

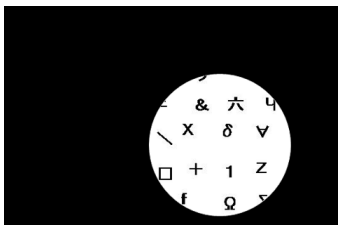

Fig. 10 Spotlight window of the spatial extent of attention (radius 30 mm). The window moves over the gaze position network.

necessarily minimized only when the gaze position network was small-world. This can be attributed to the fact that the probability of finding a target symbol [eq. (14)] may be incorrect, because it is evaluated from an actual visual search experiment in which a small-world network was assumed. If the eye continues to move quickly without stopping, then empirically, finding the target becomes more difficult. In order to estimate the correct probability of finding the target, another visual search experiment in which the eye movement is not forced to stop is needed. We are now conducting an evaluation of the probability of finding a target symbol depending on the value of q by presenting study participants with a spotlight window of the spatial extent of attention (radius 30 mm), as shown in **Fig. 10**. This window automatically moves according to the gaze position network, so that the participant is only asked if there is a target symbol in it. Through such experiment, the probability of finding the target symbol can be correctly assessed when the participants are given a target finding task with this small window moving quickly.

On the other hand, for $q < 0.014$ that is also outside the small-world range, why is a relatively long search time similar to the authors' expectations obtained? The ratio of the area scanned by the gaze position to the area of the whole search array board is defined as the *efficiency* [2]. In the range of $q < 0.014$, the number of saccades is small; consequently the *efficiency* is low and the percentage of gaze positions approaching the target symbol is small. The probability of finding the target symbol [eq. (14)] is defined only when the target symbol enters into the spatial extent of attention of the gaze position. Therefore, the relatively long search time observed for $q < 0.01$ is not due to the effect of eq. (14), but to the effect of the *efficiency*.

7. Discussion

Our research has been based on the assumption that the efficiency of a visual search is hidden in the small-world features of an unobservable gaze position network. A small-world network is conceptually defined as having a relatively large $\bar{h}(q)$ [27], where q is the ratio of the saccades. The value of $\bar{h}\left(q_{\exp}\right)$ estimated from the experimental data was almost the maximum value [**Fig. 7(b)**]. In general, however, the value of $q_{\exp}$ fluctuates depending on the experiment and the participants. In this paper, statistical analysis using Steel's test clarified that any gaze position network constructed in the range of $0.014 \leq q \leq 0.044$ should be classified as a small-world network. When the saccades comprise 1.4 to 4.4% of all the gaze steps, we regard the gaze position network as having small-world features (**Section 5**). The experimentally evaluated value of $q_{\exp} \cong 0.021$ (2.1%) was within the range of a small-world network. We conclude, therefore, that the actual eye position is observed as if moving on a small-world network, and that the network is not explicitly observed in the visual search experiment.

The eye is an organ that is inseparable from the function of looking. Fixational eye movements, which are generally classified as tremors, drifts, and microsaccades, are dedicated to the function of looking, such as in the perception of simple objects, words, and faces (so-called passive vision [51]). On the other hand, saccades are required for active vision [51] and are specialized in the function of searching rather than looking. When the eye acquired the ability to search in addition to the ability to look, 'large' saccades presumably evolved from microsaccades that are considered to contribute to the eyes' balance [52–54]. Such saccades that instantly shift the gaze position to a distant location are speculated to contribute significantly to a reduction in search time. Our artificial gaze step model showed that the search time decreased as the ratio of saccades included in the designed gaze position network increased. When the ratio of saccades reached around 2.1% (between 1.4% and 4.4%), the gaze position network became small-world and the search time was minimized. In other words, the small-world nature of the gaze position network is associated with reduced search time to find the target symbol, in a similar manner as unobservable complex human relationships reflecting the smallness of the real world. [25–27].

When the saccade ratio was further increased, however, the search time remained nearly constant at the minimum level, even though the gaze position network was no longer small-world. Such gaze position networks are composed almost entirely of saccades. There is the ability to 'search' for the target symbol, but the ability to 'look' at it is greatly diminished. Therefore, too many saccades cause an increase in search time. In order to clarify the above hypothesis, we need to estimate an appropriate probability for finding depending on the ratio of saccades, q, as described in **Section 6**. Future work will be to determine experimentally the probability of

finding, especially in the range of larger q values. To this end, we are currently conducting further experiments using the spotlight window shown in **Fig. 10**.

8. Conclusion

We implemented visual search experiments and verified the assertion that an efficient visual search can be explained by the small-world features in an unobservable network superimposed on a search array board (gaze position network). Using discriminant analysis, which is often applied to the binarization of gray scale images, we extracted saccades that satisfy the main sequence from the gaze position intervals (or gaze step). Then, using distinct gaze steps, i.e., fixational movements and saccades, we specifically designed gaze position networks. When the ratio of the saccades to the total number of line segments was close to that of the experimental data ($q \cong 0.021$), the gaze position networks became small-world by satisfying both conditions of large clustering coefficient and minimum distance between two arbitrary nodes. Additionally, simulation of the gaze position in searching for a virtual target symbol on a small-world network yielded efficient search times comparable to the experimental search times. Thus, we conclude that the small-world features hidden in gaze position networks improve the efficiency of visual searches.

In visual searches, it is generally presumed that the gaze position moves freely on the search array board to search for the target symbol. In this paper, in contrast, we hypothesized that unobservable (conceptual) networks behind the search array board control the efficiency of the visual search. We revealed that real networks designed from the experimental data are small-world. Furthermore, we simulated the search time using an artificial gaze step model and showed that the search time was minimum when the network was small-world. Thus, we have shown that the factors affecting the efficiency of a visual search can be explained from the viewpoint of complex network science such as small-world networks.

Conflict of Interest Discloser

We have no conflict of interest with any company or commercial organization.

Acknowledgments

The authors would like to thank Prof. T. Yamazaki for helpful discussion, and also to thank M. Ozawa, F. Kagaya and K. Hatta for data analyses. This work was supported by JST SPRING, Grant Number JPMJSP2121.

References

1. Amor TA, Reis SDS, Campos D, Herrmann HJ, Andrade JS Jr.: Persistence in eye movement during visual search. Sci Rep. **6**, 20815, 2016.
2. Amor TA, Lukovic M, Herrmann HJ, Andrade Jr JS: How images determine our visual search strategy. J R Soc Interface. **14**, 20170406, 2017.
3. Drew T, Boettcher SEP, Wolfe JM: One visual search, many memory searches: An eye-tracking investigation of hybrid search. J Vis. **17**(11), 5, 2017.
4. Becker SI: Determinants of dwell time in visual search: similarity or perceptual difficulty?. PLoS One. **6**(3), e17740, 2011.
5. Dewhurst R, Foulsham T, Jarodzka H, Johansson R, Holmqvist K, Nystrom M: How task demands influence scanpath similarity in a sequential number search task. Vision Res. **149**, 9–23, 2018.
6. Dube B, Basciano A, Emrich SM, Al-Aidroos N: Visual working memory simultaneously guides facilitation and inhibition during visual search. Atten Percept Psychophys. **78**, 1232–1244, 2016.
7. Watson MR, Brennan AA, Kingstone A, Enns JT: Looking versus seeing: Strategies alter eye movements during visual search. Psychon Bull Rev. **17**(4), 543–549, 2010.
8. Greene HH, Brown JM: Where did I come from? Where am I going? Functional differenced in visual search fixation duration. J Eye Movement Res. **10**(1), 10.16910/jemr.10.1.5., 2017.
9. Wasaki N, Takeuchi Y, Yoshimoto S: The effect of daily experience in gaze patterns in visual search. Vision. **31**(2), 55–66, 2019.
10. Clarke A DF, Irons JL, James W, Leber AB, Hunt AR: Stable individual differences in strategies within, but not between, visual search tasks. Q J Exp Psychol (Hove). **75**(2), 289–296, 2020.
11. Schill HM, Cain MS, Josephs EL, Wolfe JM: Axis of rotation as a basic feature in visual search. Atten Percept Psychophys. **82**, 31–43, 2020.
12. Wolfe JM: Visual search: How do we find what we are looking for? Annu Rev Vis Sci. **15**, 539–562, 2020.
13. Wolfe JM, Horowitz TS: Five factors that guide attention in visual search. Nat Hum Behav. **1**, 0058, 2017.
14. Loomis JM, Golledge RG, Klatzky RL: Navigation system for the blind. Auditory display modes and guidance. Presence. **7**, 193–203, 1998.
15. Liu X, Makino H, Kobayashi S, Maeda Y: Research of practical indoor guidance platform using fluorescent light communication. IEICE Trans Commun. **E91-B**(11), 3507–3515, 2008.
16. Maeda Y, Tani K, Ito N, Miyakawa M: Quantitative analysis on usability of button-input interfaces. IEICE Trans Fundam. **E94-A**(2), 789–794, 2011.
17. Hick WE: On the rate of gain of information. Q J Exp Psychol. **4**, 11–26, 1952.
18. Kodera R, Tanahashi S, Iijima S, Maeda Y: Measurement of eye movement in visual search for a target symbol and simulation to construct a small-world network. Adv Biomed Eng. **6**, 129–133, 2017.
19. Kodera R, Tsuno M, Ozawa M, Nomura T, Tsukada A, Maeda Y: A model of gaze migration optimizing visual search. Trans Jpn Soc Med Biol Eng. **56**(5), 190–197, 2018. (in Japanese)
20. Bao C, Kagaya F, Matsui M, Ozawa M, Nomura T, Tsukada A, Maeda Y: Small-world phenomena of gaze-point network in visual search. IEICE Trans Fundamentals. **J103-A**(7), 142–151, 2020. (in Japanese)
21. Mirman D, Irwin JR, Stephen DG: Eye movement dynamics and cognitive self-organization in typical and atypical development.

Cogn Neurodyn. **6**, 61–73, 2011.

22. Changizi M: The Vision Revolution. BenBella Books, 2009.
23. Tresselt ME, Mayzner ME: Estimates of "SVE" processing time. Psychon Sci. **16**, 103–104, 1969.
24. Libet B: Mind Time. Harvard University Press, 2004.
25. Milgram S: The small world problem. Psychol Today. **2**, 60–67, 1967.
26. Travers J, Milgram S: An experimental study of the small world problem. Sociometry. **32**(4), 425–443, 1969.
27. Watts DJ, Strogatz SH: Collective dynamics of 'small-world' networks. Nature. **393**, 440–442, 1998.
28. Liao X, Vasilakos AV, He Y: Small-world human brain networks: Perspectives and challenges. Neurosci Biobehav Rev. **77**, 286–300, 2017.
29. Strona G, Castellano C, Fattorini S, Ponti L, Gutierrez AP, Beck PSA: Small world in the real world: Long distance dispersal governs epidemic dynamics in agricultural landscapes. Epidemics, **30**, 100384, 2020.
30. Rehman A, Paul A, Ahmad A: A query based Information search in an individual's small world of social internet of things. Computer Communications. **163**, 176–185, 2020.
31. Hurst HE: Long-term storage capacity of reservoirs. Transactions of American Society of Civil Engineers. **116**(13), 770–799, 1951.
32. Aştefănoaei C, Pretegiani E, Optican LM, Creangă D, Rufa A: Eye movement recording and nonlinear dynamics analysis – The case of saccades. Rom J Biophys. **23**(1–2), 81–92, 2013.
33. Marlow CA, Viskontas IV, Matlin A, Boydston C, Boxer A, Taylor RP: Temporal structure of human gaze dynamics is invariant during free viewing. PLoS One. **10**(9), e0139379, 2015.
34. van der Geest JN, Frens MA: Recording eye movements with video-oculography and scleral search coils: a direct comparison of two methods. J Neurosci Methods. **114**(15), 185–195, 2002.
35. Hsiao JH, Cottrell: Two fixations suffice in face recognition. Psychol Sci. **19**(10), 998–1006, 2008.
36. Crabb DP, Smith ND, Rauscher FG, Chisholm CM, Barbur JL, Edgar DF, Garway-Heath DF: Exploring eye movements in patients with glaucoma when viewing a driving scene. PLoS One. **5**(3), e9710, 2010.
37. Zemblys R, Niehorster DC, Holmqvist K: gazeNet: End-to-end eye-movement event detection with deep neural networks. Behav Res Methods. **51**(2):840–864, 2019.
38. Krishnamoorthy A, Sindhura VR, Gowtham D, Chandran J, Vidyapeetham AV: StimulEye: An intelligent tool for feature extraction and event detection from raw eye gaze data. Journal of Intelligent and Fuzzy Systems. **41**(5), 5737–5745, 2021.
39. Takagi M, Shimoda H (eds.): Handbook of Image Analysis. University of Tokyo Press, p. 503, 1991.
40. Bahill AT, Clark MR, Stark L: The main sequence, a tool for studying human eye movements. Math Biosci. **24**, 191–204, 1975.
41. Shioiri S, Ikeda M: Useful resolution for picture perception as a function of eccentricity. Perception. **18**(3), 347–361, 1989.
42. Yu D, Legge GE, Wagoner G, Chung STL: Training peripheral vision to read: boosting the speed of letter processing. Vision Res. **152**, 51–60, 2018.
43. Xiong YZ, Qiao C, Legge GE: Reading with letter transpositions in central and peripheral vision. J Vis. **19**(3), 17, 2019.
44. Stewart EEM, Valsecchi M, Schutz AC: A review of interactions between peripheral and foveal vision. J. Vis. **20**(12), 2, 2020.
45. Tanrikulu OD, Chetverikov A, Kristjansson A: Encoding perceptual ensembles during visual search in peripheral vision. J. Vis. **20**(8), 20, 2020.
46. Trouilloud A, Kauffmann L, Roux-Sibilon A, Rossel P, Boucart M, Mermillod M, Peyrin C: Rapid scene categorization: From coarse peripheral vision to fine central vision. Vision Res. **170**, 60–72, 2020.
47. Wu CC, Wolfe JM: The functional visual field(s) in simple visual search. Vision Res. **190**, 107965, 2022.
48. Palmer J, Moore CM: Using a filtering task to measure the spatial extent of selective attention. Vision Research. **49**, 1045–1064, 2009.
49. Shioiri S, Honjo H, Kashiwase Y, Matsumiya K, Kuriki I: Visual attention spreads broadly but selects information locally. Sci Rep. **6**, 35513, 2016.
50. Dijkstra EW: A note on two problems in connexion with graphs. Numerische Mathematik. **1**, 269–271, 1959.
51. Findlay JM, Gilchrist ID: Active Vision: The Psychology of Looking and Seeing. Oxford University Press, 2003.
52. Engbert R, Kliegl R: Microsaccades keep the eyes' balance during fixation. Psychol Sci. **15**(6), 431–436, 2004.
53. Laubrock J, Engbert R, Kliegl R: Microsaccade dynamics during covert attention. Vision Res. **45**, 721–730, 2005.
54. Engbert R, Mergenthaler K, Sinn P, Pikovsky A: An integrated model of fixational eye movements and microsaccades. Proc Natl Acad Sci. **108**, E765–E770, 2011.

Yuxuan WANG

Yuxuan WANG received a B.E. (2016) in Graduate School of Electrical and Information Engineering from Northeast Petroleum University, Daqing, China. She received a M.E. (2021) in Graduate School of Science and Technology from Niigata University, Niigata, Japan. She is currently pursuing the Ph.D. degree in Electrical and Information Engineering with the Niigata University, Niigata, Japan. Her research fields are medical and biological engineering and information engineering. She is a student member of IEICE.

Honami HASHIMOTO

Honami HASHIMOTO received a B.E. (2021) in Faculty of Engineering from Niigata University. She is currently studying in Graduate School of Science and Technology, Niigata University. Her research fields are biometric information systems.

Taishin NOMURA

Taishin NOMURA received his BSc degree from the Department of Physics, and MSc and PhD degrees from the Department of Biophysical Engineering at Osaka University, Japan. He was a postdoctoral researcher at Centre for Nonlinear Dynamics in Physiology and Medicine at McGill University from 1995 to 1996. Since 2004, he has been a full professor at the Graduate School of Engineering Science at Osaka University. His research interests include motor control during bipedal stance and gait in health and disease, with emphasis on stability flexibility tradeoff. He is a regular member of SICE, IEICE, JSMBE and JSCB.

Akira TSUKADA

Akira TSUKADA received his M.E. degree from Toyama University (1987), and Ph.D. degree from Osaka University (1999). He worked at Arimura Institute of Technology (1987–1991). He was Research Associate at Toyama University (1991–2002), Associate Professor at National Institute of Technology, Toyama College (2002–07), and presently, Professor at Department of Electronics and Computer Engineering, National Institute of Technology, Toyama College. His current research interests include virtual facial expression analysis and human interface. He is a regular member of JSMBE, ITE and IEICE.

Yoshinobu MAEDA

Yoshinobu MAEDA received a M.E. (1995) and a Ph.D. (1998) in Graduate School of Engineering Science from Osaka University. He was JSPS Research Fellow in Osaka University (1995–98), Research Associate in Niigata University (1998–2005), Associate Professor in Niigata University (2005–15), and presently, Professor in Graduate School of Science and Technology, Niigata University. His research fields are analyses of neuro-dynamics and socio-dynamics, human interface designs in assistive technologies, etc. He is a regular member of JSMBE, JSWSAT, IEE of Japan, and a senior member of IEICE.